Paper 104

Proceedings of the Eleventh International Conference
on Computational Structures Technology,
B.H.V. Topping, (Editor),
Civil-Comp Press, Stirlingshire, Scotland

Fatigue Assessment of a Riveted Plate Girder Railway Bridge: Numerical and Experimental Investigations

V. Zabel, A. Schmidt and I. Reichert
Institute of Structural Mechanics
Bauhaus-University Weimar, Germany

Abstract

Usually the structural safety of existing bridges is performed based both on calculations and regular inspections. Respective numerical procedures for the estimation of remaining lifetime are described in national and international guidelines.

Within the study described here, a riveted plate girder bridge was considered. The structure was erected in the early 1930s. Even though the structure is generally in a good condition, few local cracks were identified by visual inspections. One of these cracks is located in a gusset plate. This observation was the starting point for further investigations which are described in this contribution.

First a finite element model of the superstructure was created. To verify that the model represents the global structural behaviour of the bridge with sufficient accuracy an experimental modal analysis was performed. Based on the measured data several natural frequencies and mode shapes were identified.

In a next step the expected remaining lifetime of the main structural elements was estimated based on a standard approach. The results propose a remaining lifetime of several decades. From numerical simulations of a train passage the cracked gusset plate was identified as a hot spot with the highest stress concentrations in the structure. This gave reason to further investigations that concentrate on this structural detail. An assessment of this critical structural detail according to a standard method gave the result that the nominal lifetime of this local structural element has already expired.

Further investigations include a structural health monitoring system that controls both the actual loads by passing trains and the resulting strains in the considered gusset plate. Based on the monitored loads the assumptions for the calculations can be improved. Furthermore the calculated stresses can be validated by comparison with measured data. The two latter questions are subject of ongoing research.

Keywords: fatigue assessment, steel railway bridge, structural health monitoring.

1 Introduction

Fatigue of steel railway bridges has been a research field for many years. As a result structural details are nowadays usually designed such that fatigue should be a problem of minor importance for new bridges. However, for older bridges this is not always the case. During bridge inspections cracks that may have been caused by fatigue are detected occasionally. In these situations always arises the question of remaining life expectancy.

The estimation of the remaining lifetime of an existing railway bridge is usually performed by means of calculations according to respective guidelines such as [1], [2], and [3]. If a sufficient level of structural safety cannot be proofed alone by numerical analyses, the option of additional experimental investigations is foreseen for example in [2].

Due to the large variety of structural details the specific problems in individual structures can be very different. Accordingly a standardized approach for a measurement-based fatigue assessment of existing structures has not been included in the guidelines. This gave reason for systematic investigations of currently applied approaches and the development of experimental procedures for fatigue assessment of existing steel bridges within a European research project.

In this project several numerical and experimental investigations have been performed for different case studies. One of these case studies is described in this paper. The research is still in progress, Nevertheless some of the applied approaches and respective results can already be presented in the following sections.

2 Description of the considered bridge

One very typical type for steel railway bridges, erected in the first half of the 20th century, is the riveted plate girder type. The main girders of these bridges usually have an I-section. The webs consist of metal sheet that is connected to the flat steel bars of the flanges by angular sections and rivets. Often the geometry of the cross section, e.g. the height of the web or the thickness of the flanges, follows the size of the internal forces along the beam axis. Typically these bridges were used for spans from 5 to 40 m.

Between the main girders the cross beams span in lateral direction which carry the longitudinal beams that support the sleepers. In many cases the tracks are situated between the two main girders. There are bridges with ballast laying on curved metal sheets while in other cases the sleepers are directly connected to the steel structure.

The bridge under consideration here is the Saalebrücke Großheringen. It is situated near Naumburg in central Germany and is part of the main connection Berlin – Munich. The bridge was constructed between 1932 and 1935. It consists of five 35 m to 40 m long spans. Each of these spans consists of a simply supported riveted plate girder superstructure. The two tracks are accommodated on separated super-

Figure 1. Saalebrücke: complete aspect (top), considered plate girder span (bottom left), view from underneath the bridge (bottom right).

structures. The 75 m long opening over the river Saale is bridged by simply supported riveted truss girders. The whole bridge is situated in a curve which is the reason for a speed limitation of the rail traffic to 90 km/h.

Since most of the superstructures are designed and constructed in a very similar way it is concentrated on a single span which can be considered as being representative for all plate girder superstructures of this bridge. For the investigations within the research presented here, the most northern end span of the bridge was selected. It carries the southbound track and is a typical example for a riveted plate girder bridge. Figure 1 shows photographs of the bridge.

During a bridge inspection a crack was identified in a gusset plate which could be caused by fatigue. Even though this crack is of secondary importance for the structural safety of the whole bridge, a further investigation has been considered as an interesting case study. It has been assumed that the crack in the gusset plate occurred due to stress concentrations in the respective connection caused by distortions of the cross beam during the passage of trains, i.e. distortion induced fatigue. The respective distortions can be generated due to the eccentric connection of the longitudinal beams, which carry the sleepers, to the cross beams which leads to torsion in the cross beam. Furthermore the crack is situated at a location with a sharp change of stiffness.

3 Numerical models of the structure

3.1 Finite element model for preliminary studies

To obtain a first overview of the global structural behaviour of the bridge under consideration a relatively simple finite element model was created. This model was formed by beam elements with respective cross sections and material properties of the main girders, the cross beams, the longitudinal beams and the main lateral bracings. With this model the natural frequencies and mode shapes of the lowest modes, which are also supposed to be the most relevant in the context of fatigue, were calculated. In figure 2 the first three calculated global mode shapes and natural frequencies are summarized.

As the considered structure consists of many slender structural elements, such as the bracings, it was expected, that also local modes of specific elements could have an influence on vibration induced fatigue. These effects could not be represented sufficiently well by the first finite element model. Additionally a numerical model was needed that allows the calculation of local structural stresses. This gave reason for the creation of a more refined finite element model.

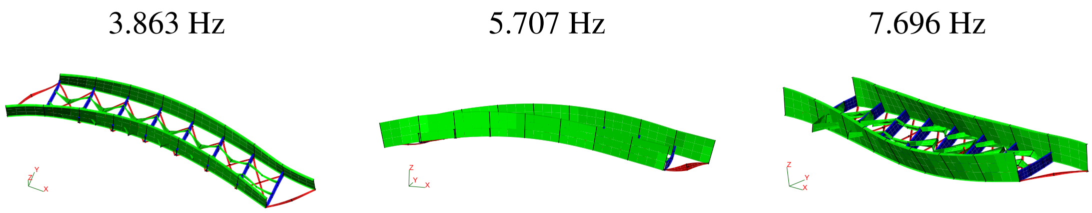

Figure 2. First model consisting of beam elements: first three calculated global modes.

3.2 Finite element models for numerical simulations

A more detailed finite element model of the complete superstructure of the bridge's end span was created in several stages. In the first refined model all primary steel members were modelled by 4 node shell elements. A graphic representation of this model is shown in figure 3.

To identify locations of concentrated stresses under live load, the movement of a constant vertical axel load along the longitudinal beams was simulated by means of the first refined model. The axel load was placed at several positions along the track. For each loading location the static response of the structure was computed. Figure 4a) indicates the von Mises stresses for load locations close to the cross beam that is connected to the main girder at the support. An interesting finding is that there is a significant stress concentration at the connection of the cross beam to the main girder. The influence line of the stresses at the location of the stress concentration

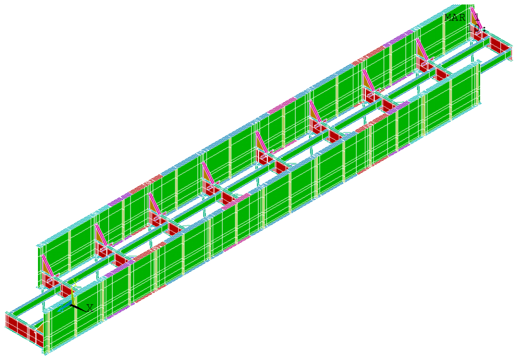

Figure 3. Second model consisting of shell elements.

a) b)

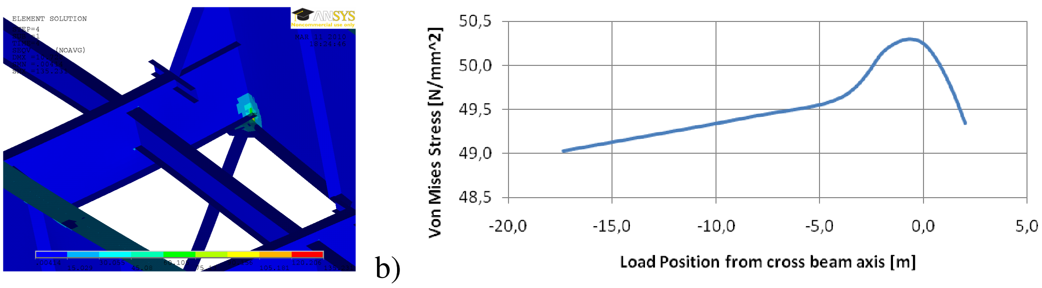

Figure 4. a) Stress concentrations at the connection of cross beam and main girder at the pier support, b) influence line of von Mises stresses at the hot spot with respect to the load's distance from the cross beam's axis.

with respect to the distance of the axel load to the cross beam is given in figure 4b). In this curve the maximal stresses occur shortly before the axel reaches the axis of the cross beam. This observation supports the hypothesis that an eccentric loading on the cross beam results in torsion of the cross beam which leads to stress concentrations in the respective structural connection.

The described results supported the initial assumption that the identified crack in the gusset plate was caused by fatigue due to cyclic loading during the passages of trains. Nevertheless a further refinement of the model in the surroundings of the considered gusset plate was required for a detailed stress analysis. Therefore the elements around the respective support on the pier were re-meshed such that the true geometry of this detail was represented with sufficient accuracy as illustrated in figure 5. Additionally secondary elements such as the bracings between the longitudinal beams and the stiffeners of the main girders' webs in the end fields were added.

This model allowed also for the representation of the local modal behaviour. The first 100 calculated modes clearly show that the majority are local rather than global modes. This means that most modes are characterized by vibrations of several structural elements such as web plates of the main girders or bracings. The first three global

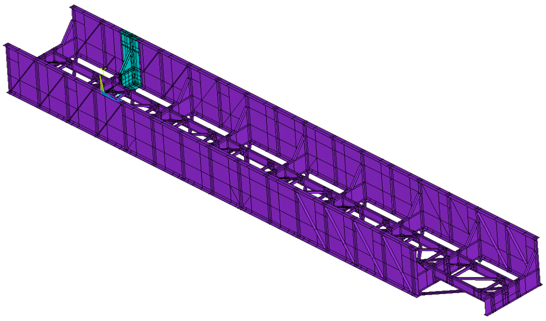

Figure 5. Third model consisting of shell elements, including secondary structural members and refinement of the considered detail.

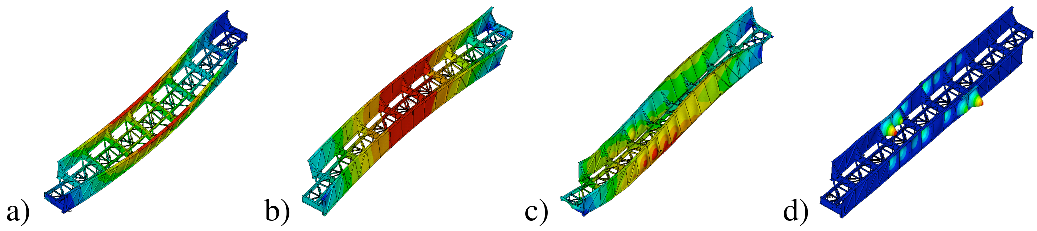

Figure 6. Third FE-model: first three global mode shapes – a) to c), example for a local mode shape characterized by web plate bending – d).

mode shapes and an example for a local mode shape which is characterized by plate bending of the web are shown in figure 6.

As a result of the simulation of the passage of a heavy locomotive the stress distribution illustrated in figure 7 was obtained for the moment when a boogie passes the cross beam at the support. It can be clearly seen that there are highly concentrated stresses in the gusset plate at the location of the crack, i.e. at the end of the cross beam's bottom flange. These calculations also confirmed the hypothesis that the identified crack in the gusset plate was caused by fatigue.

4 Experimental modal analysis

To verify the numerical models of the considered span, dynamic tests were performed to identify the modal parameters of the superstructure. Due to reasons of accessibility 3D accelerometers were only placed on the upper flanges of the main girders. Since not all measurement points could be instrumented at the same time, the measurements with ambient excitation were performed with three setups using two 3D reference sensors. An additional accelerometer was installed on the upper flange of one main girder of the adjacent span to obtain initial information about modal coupling of these two superstructures which are statically decoupled. The locations of the measurement

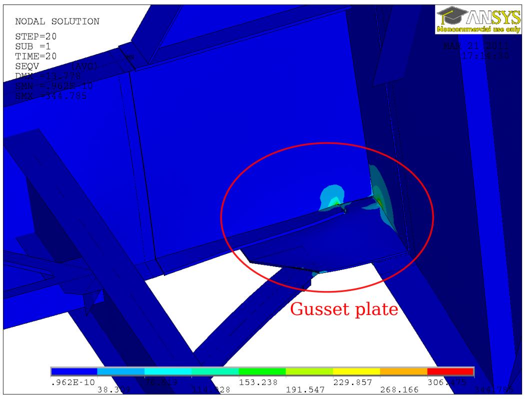

Figure 7. Stress concentrations calculated for the considered detail during the passage of a heavy locomotive.

points in plan are given in figure 8.

From the measured time series the five modes illustrated in table 1 were identified using the covariance-driven reference-based Stochastic Subspace Identification (SSI-cov/ref) method [4]. Data preprocessing, system identification and modal analysis were performed using the MATLAB toolbox MACEC, developed by the Structural Mechanics division of K.U. Leuven [5]. Three of the five identified modes are clearly corresponding, both in shape and frequency, to the first three global modes calculated with the finite element models shown in figure 2. However, two further identified modes showed almost only movements of the measurement point in the second span. These observations gave reason to the assumption, that these modes could be a lateral and a vertical bending mode of the second span's superstructure. This assumption could be confirmed by a more extensive test campaign that also included the consideration of local modes [6].

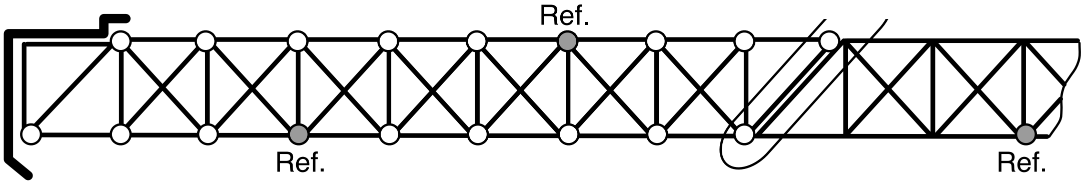

Figure 8. Measurement points on the upper flanges for the dynamic tests.

nat. frequency damping ratio	description	image
$f_1 = 3.60\ Hz$ $\zeta_1 = 0.71\,\%$	first lateral bending mode of span 1	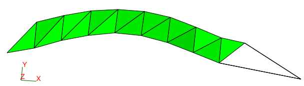
$f_2 = 4.16\ Hz$ $\zeta_2 = 2.15\,\%$	first lateral bending mode of span 2	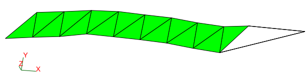
$f_3 = 5.26\ Hz$ $\zeta_3 = 1.26\,\%$	first vertical bending mode of span 1	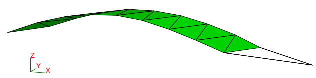
$f_4 = 5.84\ Hz$ $\zeta_4 = 2.87\,\%$	first vertical bending mode of span 2	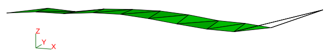
$f_5 = 7.91\ Hz$ $\zeta_5 = 3.41\,\%$	first torsional mode of span 1	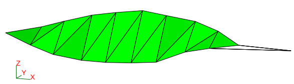

Table 1. First five global modes identified from the first test campaign.

5 Estimation of remaining lifetime by numerical analyses

Usually an estimation of remaining lifetime of existing structures is performed based on numerical analyses. A methodology that has to be applied in practical applications to existing steel railway bridges in Germany is described in guideline 805 of Deutsche Bahn (DB, German Railways) [2]. The standard approach is devided into four steps:

1. **Calculation of the fatigue relevant coefficient for the loading capacity** $\beta_{\mathrm{D,UIC}}$:

$$\beta_{\mathrm{D,UIC}} = \frac{\mathrm{zul}\Delta\sigma_{\mathrm{Be},\kappa}}{\gamma_{\mathrm{B}} \cdot \Theta \cdot \max\sigma_{\mathrm{UIC}}} \tag{1}$$

where

Θ	...	dynamic amplification factor,
$\mathrm{zul}\Delta\sigma_{\mathrm{Be},\kappa}$	...	permitted value of the double amplitude of the stress in $\mathrm{N} \cdot \mathrm{mm}^{-2}$ under consideration of the notch type, the material and the ratio of stresses κ and
γ_{B}	...	partial safety factor for the structural condition (considering corrosion).

$$\kappa = \frac{\sigma_{\mathrm{G}} + \Theta \cdot \min\sigma_{\mathrm{UIC}}}{\sigma_{\mathrm{G}} + \Theta \cdot \max\sigma_{\mathrm{UIC}}} \tag{2}$$

with

σ_{G}	...	stress in $\mathrm{N} \cdot \mathrm{mm}^{-2}$ from dead load,
$\min\sigma_{\mathrm{UIC}}$	...	minimal stress in $\mathrm{N} \cdot \mathrm{mm}^{-2}$ from traffic load UIC 71 (LM71 from EN 1991-2) and
$\max\sigma_{\mathrm{UIC}}$	...	maximal stress in $\mathrm{N} \cdot \mathrm{mm}^{-2}$ from traffic load UIC 71.

2. **Calculation of the total damage of the past for the reference year 1876 (fictive damage)**:

$$D_{\mathrm{Verg,1876}} = \alpha \cdot \left(\frac{1}{\beta_{\mathrm{D,UIC}}}\right)^5 \tag{3}$$

where

$D_{\mathrm{Verg,1876}}$	...	accumulated damage sum caused by traffic from the past to the year 1996 for non-welded structures for the fictive year of construction 1876 and a yearly gross tonnage of 25×10^6 t and
α	...	coefficient depending on the decisive length l from [7].

3. **Calculation of the damage for the time period since first operation with underlying values of precise traffic conditions (precise damage)**:

$$D_{\mathrm{Verg}} = \rho_1 \cdot \rho_2 \cdot \rho_3 \cdot \rho_4 \cdot D_{\mathrm{Verg,1876}} \tag{4}$$

with

ρ_1 ... correction factor to consider the construction year of the bridge,

ρ_2 ... correction factor to consider the yearly gross tonnage per track $\rho_2 = \dfrac{t_{\text{brutto}}}{year} \cdot \dfrac{1}{25 \times 10^6\ \text{t}}$,

ρ_3 ... correction factor for multiple-tracks with the estimation of a meeting rate of 12.5% depending on the ratio of stresses $a = \dfrac{\Delta\sigma_1}{\Delta\sigma_{1+2}}$ and

ρ_4 ... correction factor to consider the permitted train speed.

4. **Calculation of the service life expectancy**:

$$R = \frac{1 - D_{\text{Verg}}}{0,01 + D_{\text{Zuk}}} - A \leq 50 \text{ years} \tag{5}$$

where

D_{Zuk} ... annual accumulated damage in the future and

A ... difference between the current year and the year 1996.

In case that measures to enhance or strengthen the structure are taken D_{Zuk} is calculated as

$$D_{\text{Zuk}} = 0,025 \cdot \frac{\rho_{2,\text{Zuk}}}{\rho_{2,\text{Verg}}} \cdot \frac{\rho_{4,\text{Zuk}}}{\rho_{4,\text{Verg}}} \cdot \left(\frac{\beta_{\text{D,UIC,Verg}}}{\beta_{\text{D,UIC,Zuk}}}\right)^5 \cdot D_{\text{Verg}} \tag{6}$$

These four steps of the standard approach were applied to both the main structural members of the superstructure and the gusset plate that was identified to be critical with respect to fatigue action by numerical investigations. Due to a lack of information about the loads that were applied to the bridge in the past, the correction factor ρ_2 was set to 1. This assumption is considered as conservative since recent monitoring results suggest considerably lower tonnage than 25×10^6 t. The results of the calculations following the standard approach given in [2] are summarized in table 2.

Structural element	max/min σ_{UIC} [N/mm^2]		$\beta_{\text{D,UIC}}$	κ	D_{Verg}	D_{Zuk} [$\times 10^{-3}$]	R [years]
Longitudinal beam	68.58	0.00	1.204	0.036	0.052	1.31	70
Cross beam	90.94	0.00	0.964	0.075	0.158	3.94	45
Main girder	90.22	0.00	1.120	0.139	0.075	1.88	61
Detail: Gusset plate	170.00	0.00	0.681	0.027	0.904	15.80	−12

Table 2. Estimated remaining lifetime R for the year 2012 and the considered structural elements according to [2].

The results in table 2 show that all main structural components have a remaining service life expectancy of more than 30 years. On the contrary the calculations for the gusset plate result in a negative remaining life expectancy, which means that the life time has already expired. This result agrees with the identification of the crack at the existing structure.

6 Monitoring system

6.1 Description of the monitoring system

To obtain more realistic information about the structure under service conditions a monitoring system was installed. In detail the main objectives for the monitoring system were defined as

- acquisition of the real axle loads of passing trains as base for prospective calculations,
- measurement of the strains in the cracked gusset plate during train passages,
- observation of the global dynamic behaviour of the superstructure and
- observation of the local dynamic behaviour of structural elements connected to the gusset plate.

Based on these major objectives respective sensor types and their locations were chosen. For the estimation of the axle loads strain gauges were placed on the rail over the abutment of the bridge. Over the first pear, at known distance from the strain gauges on the rail over the abutment, further strain gauges were installed to acquire data that allows for the estimation of speed and acceleration of passing trains.

A strain gauge rosette was placed close to the crack tip on the afore mentioned gusset plate. For comparison reasons an identical strain gauge rosette was installed on the structurally identical gusset plate over the second bearing on the first pear. Temperature sensors were installed next to the two strain gauge rosettes and at a location on the bottom side of the upper flange of the main girder.

Both the natural frequencies of the two adjacent superstructures and of the bracing connected to the considered gusset plate are identified from measured data acquired by means of geophones. In total six geophones were installed at two locations on the main girders and on the bracing measuring in lateral and vertical direction, respectively.

To minimize the possibility of noise contamination of the analogue signals, a monitoring system was chosen that digitizes the signals at node modules close to the sensors. These acquisition nodes, that host the measurement modules, are connected to a controller via ethernet. The locations of both the decentralized nodes and the sensors are shown in figure 9.

For the electric power supply of the whole monitoring system a connection to the public electricity network was provided. For the data transfer to a central server, the monitoring system was connected to a DSL telephone line.

The acquired data is transferred daily to a central server. First analyses are performed automatically to obtain a brief information about the general quality of the data and to identify defects such as sensor failures or other technical breakdowns. The results of these analyses are visualized on a web page that can be accessed by authorized users (figure 10).

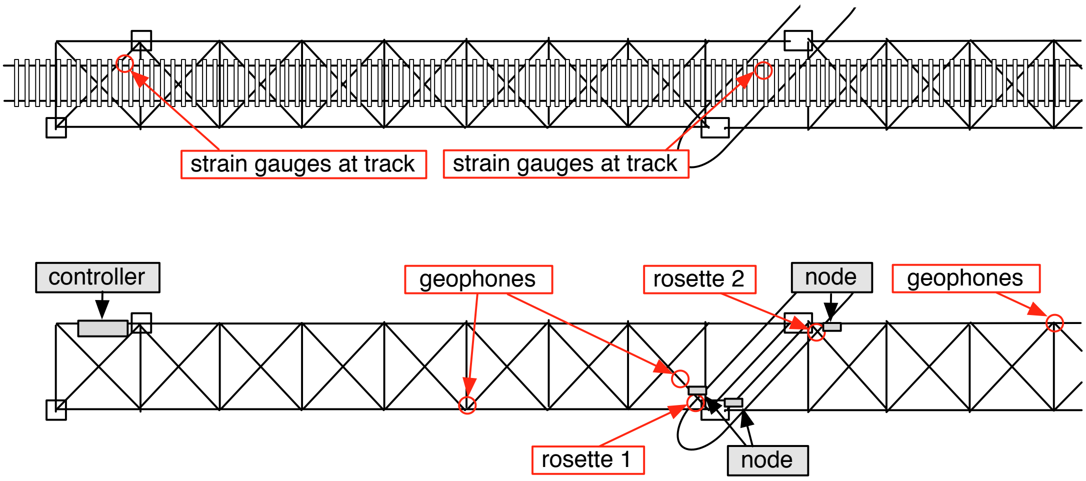

Figure 9. Scheme of locations of sensors and measurement modules of the monitoring system.

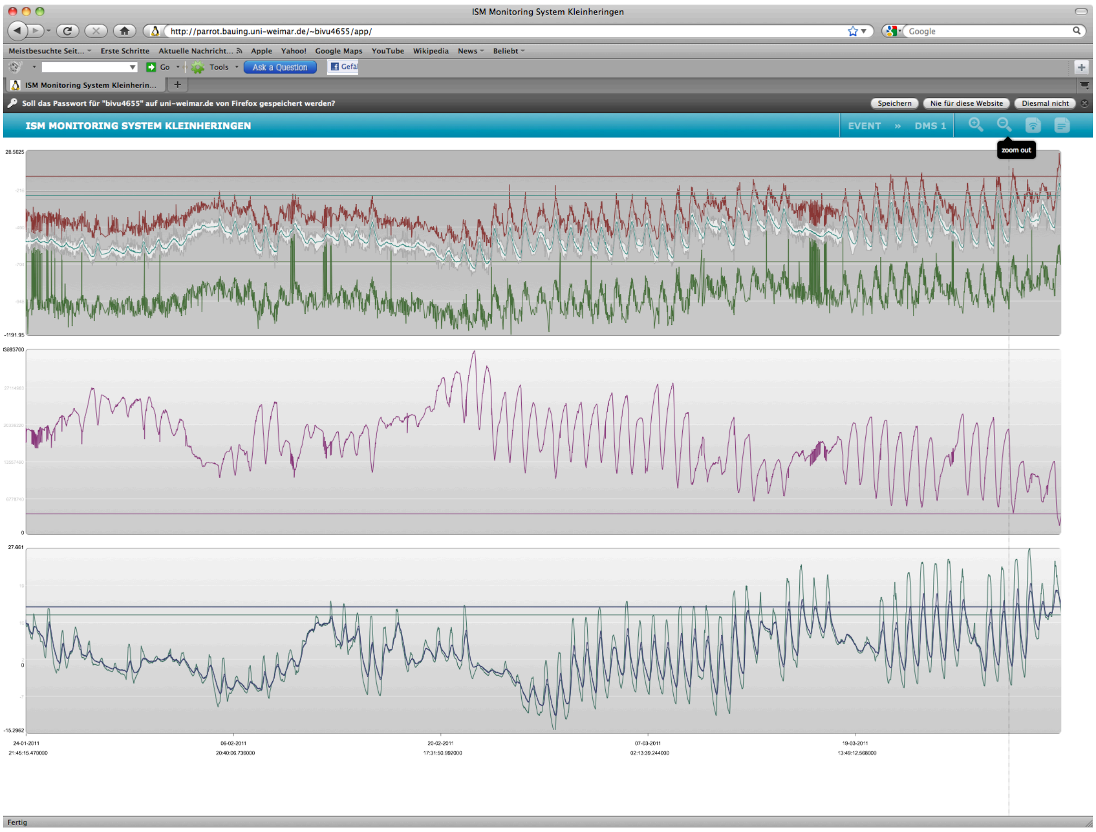

Figure 10. Web interface for the control of the monitoring system.

6.2 Selected observations obtained from the monitoring

The monitoring of the structure is part of ongoing research. Therefore the assessment of all data acquired by the monitoring system during a period of one year has not been finished yet. Nevertheless some observations that were made by analyzing the measured data are presented and discussed here.

6.2.1 Identification of train types, speed and acceleration

Using the strains measured on the rail over the abutment and over the pier, the average speed of each axle can be estimated. For this purpose an algorithm was developed that detects corresponding peaks in the two measured signals and calculates the average speed of each axle during its passage of the considered superstructure based on the extracted time lag between two corresponding peaks and the known distance between the two measurement locations. Figure 11 shows a time series of measured strains at one location at the track together with the derived average speeds for the axles. From this diagram the increasing speed of the train can be well observed.

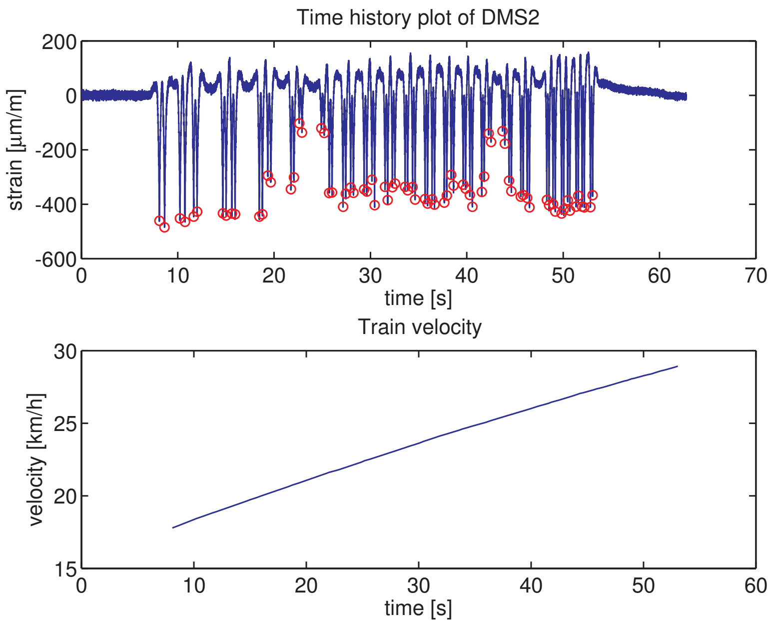

Figure 11. Time series of measured strains at a track during a train passage (top) and corresponding average axle speeds (bottom).

After calculating the speed of each axle, the distances between all axles can be derived. Based on knowledge about the axle patterns for some typical vehicles, such as locomotives and waggons used for passenger trains such as ICE, Intercity and double decker trains, the respective train type can be identified. Figure 12a) summarizes the relative occurrences of the detected train types in one year based on more than 16,000 detected trains. The diagram shows that the majority of trains passing the bridge are

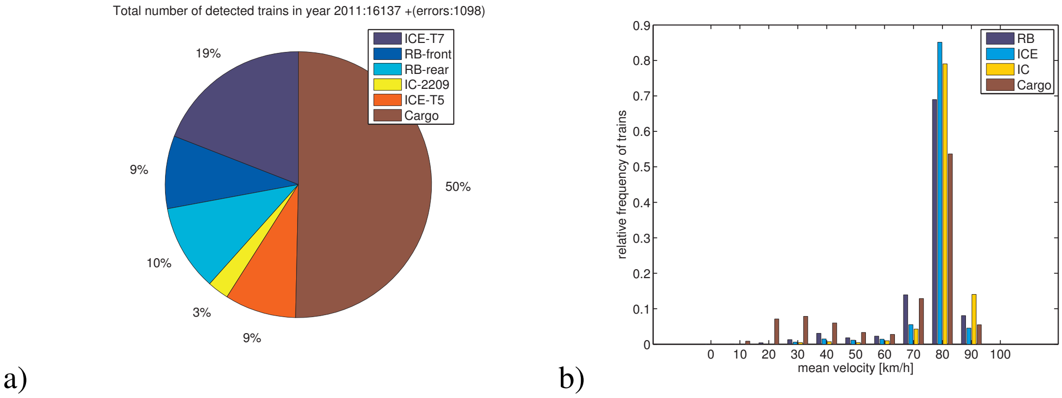

Figure 12. Identification of passing trains in one year: a) distribution of identified train types, b) speed histogram showing the relative frequency for different train types.

freight trains. Figure 12b) confirms that most trains pass the bridge at a speed of 80 to 90 $\mathrm{km/h}$, i.e. close to the speed limit. Only a small number of trains travels at comparatively low speeds, especially freight trains, mostly after having stopped at a rail signal in front of the bridge such as the train for which the diagrams in figure 11 were recorded.

6.2.2 Estimation of axle loads

The wheel loads were estimated based on strain measurements on one rail close to the abutment. For the estimation of the axle load it is assumed that the derived wheel loads are the same for one axle. Accordingly, the estimated wheel loads are doubled to derive the respective axle load. Due to the fact that the axle loads are derived from measurements of strains in the rail during train passages, the results are also influenced by dynamic effects. Several vehicle types regularly pass the bridge, such as regional trains with double decker waggons and a locomotive of type BR 143, which makes statistical assessments possible.

For locomotives the nominal axle loads can be extracted from respective data sheets such as [8]. This gives a very good opportunity to assess the estimated axle loads. Figure 13a) summarizes all estimated mean axle loads which were calculated as the average of the four respective values identified for each locomotive of type BR 143 with respect to train speed. The boxes mark the range from 25 % to 75 % of all respective mean values of the four locomotive axles. From the diagram can be derived that for speeds up to $70\mathrm{km/h}$ the identified average axle loads coincide well with the nominal axle load of 210 kN with a deviation range of approximately $\pm$ 5 %. For higher speeds the average mean axle loads tend to decrease, while the scatter of the mean axle loads increases. This observation gives reason to assume that dynamic effects such as bridge–vehicle interactions have an increasing influence on the axle load estimates with increasing train speed.

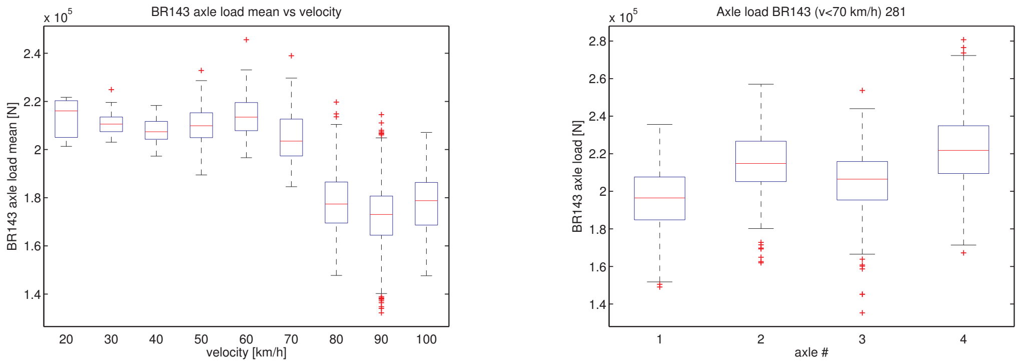

a) b)

Figure 13. Axle load identification: a) statistics of the mean values of the identified axle loads of the locomotives of type BR 143 with respect to speed, b) statistics of the identified axle loads for the four axles of locomotives of type BR 143 with speeds up to $70\mathrm{km/h}$; the boxes include all samples from 25 to 75 %, the dashed lines extend to the most extreme data points not considered as outliers, outliers are plotted individually (red cross).

Another observation that was made for the majority of vehicles, such as locomotives, that have boogies with two axles, is that the load identified for the respective second axle was usually slightly higher than the one corresponding to the first axle of the boogie. Figure 13b) illustrates the statistics of the identified axle loads for all detected locomotives of type BR 143 with a speed of up to $70\mathrm{km/h}$. The boxes mark the range from 25 % to 75 % of all respective samples for one axle. The observed deviations of axle loads between adjacent axles agree with the assumption that the longitudinal force that has to be generated to move the train leads to an additional moment about the boogie's lateral axis and consequently to differences between the vertical forces transmitted through the wheels. Respective theoretical derivations were developed for example in [9].

6.2.3 Local strain measurements

Local strains were measured with two strain gauge rosettes on two identical gusset plates over the pier. From the measured time series the von Mises effective stresses were calculated. Subsequently rainflow counting was applied to the von Mises stresses. Stress cycles with amplitudes of less than $10\mathrm{N/mm^2}$ were excluded from the rainflow statistics.

As clearly shown in figure 14 for a period of four months, especially load cycles at higher stress levels are associated with passing freight trains. This observation can be expected due to the higher loads of freight trains. A comparison of the cycles of von Mises stresses counted for the two locations on the gusset plates shows that the stresses in the two identical structural elements are different (figure 15). It can be observed that the numbers of cycles with higher stress amplitudes obtained for strain

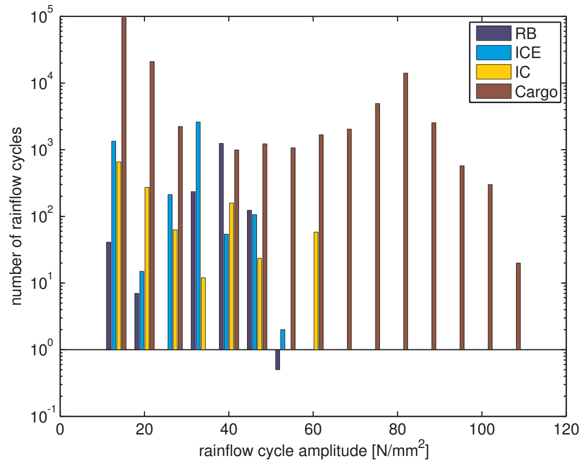

Figure 14. Rainflow historgram of von Mises stresses calculated from strains measured with strain gauge rosette on the cracked gusset plate over a period of four months grouped for different train types.

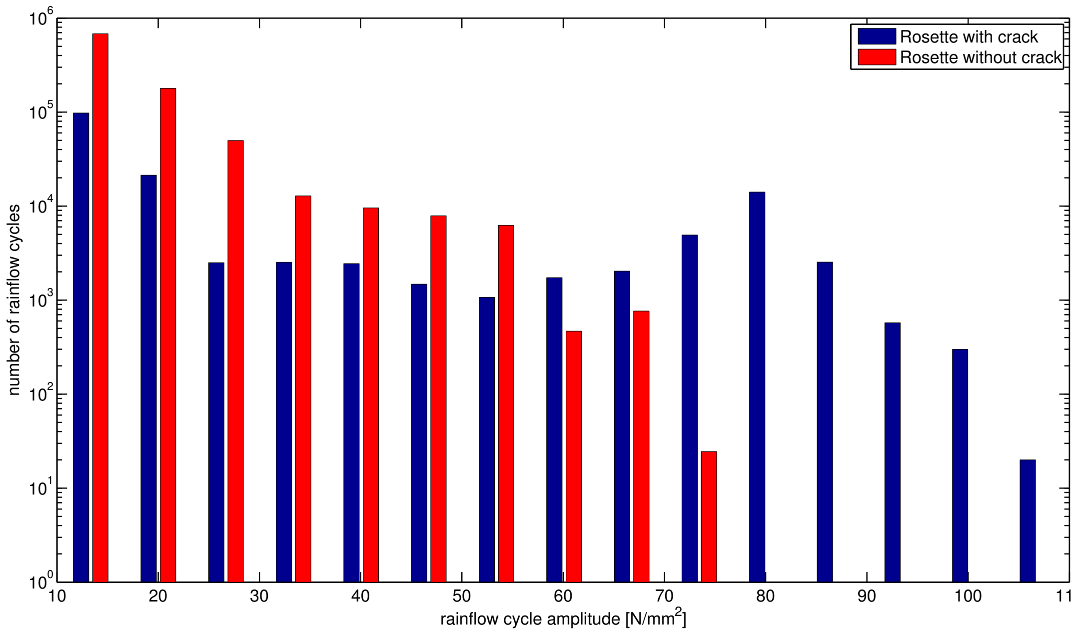

Figure 15. Von Mises stresses – rainflow histogram of the strain gauge rosettes on the gusset plates with (blue) and without crack (red) for four months.

gauge rosette 1, which is situated in front of the crack tip on the damaged gusset plate, are larger than for rosette 2 on the non-damaged gusset plate. This result justifies the assumption of higher stresses in the cracked gusset plate close to the crack due to resulting stress re-distributions.

Using the S/N curve 71 from [10] for the gusset plate detail of the bridge damage numbers of $D_1 = 0.78$ and $D_2 = 0.08$ can be calculated for the respective time period of four months according to Palmgren-Miner rule for rosette 1 (with crack) and rosette 2 (without crack), respectively.

7 Laboratory fatigue tests of the detail gusset plate

As described in section 5 the fatigue life expectancy of the critical detail expired already as can be assumed also by the presence of the crack in the real structure. This finding is also supported by the numerical results described in section 3.2 that showed stress concentrations at the location of the identified crack.

By means of laboratory fatigue tests S/N curves will be derived to improve the estimations of damage accumulation due to fatigue and resulting remaining life time expectancies for this detail. To prepare the design of the laboratory tests, first a loading situation had to be defined that

- leads to a similar stress distribution as in the gusset plate on the bridge and
- can be generated with reasonable technical effort in the laboratory.

After an iterative process of investigations considering different boundary conditions, loading locations and directions, a configuration was found that allows for the application of a unidirectional load. Figure 16a) shows the numerical model of the gusset plate while in figure 16b) the stress distribution is given if translational displacements along line L8 are applied to the plate which is fixed along lines L1, L2 and L9. The stress distributions are very similar to those calculated for the gusset plate in the bridge model during a train passage.

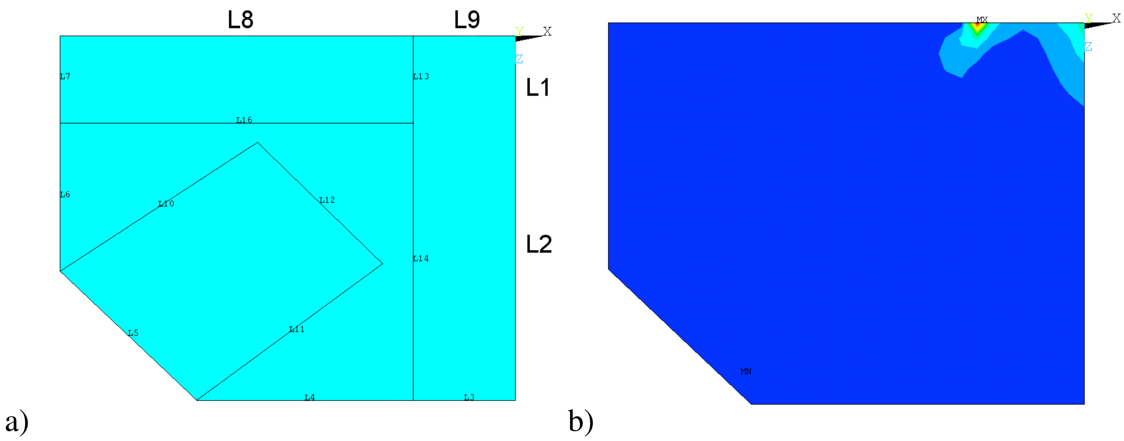

Figure 16. Numerical model of the gusset plate: a) geometry, b) stress distribution due to translational displacements along line L8.

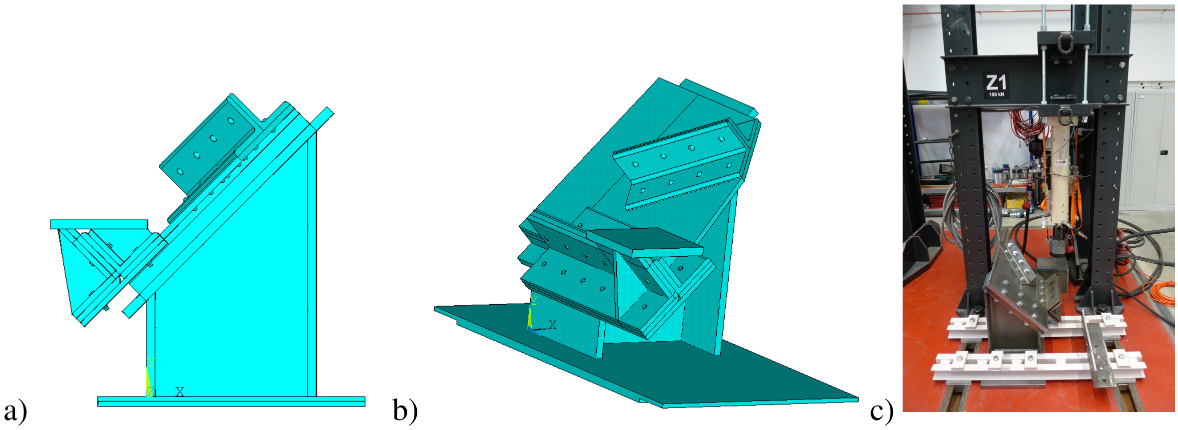

Figure 17. Setup for fatigue tests: a) model – side view, b) model – isometric view, c) test bed in the laboratory.

Based on these results an experimental setup was developed. The assumed displacements along line L8 in figure 16a) were not in the direction of one global coordinate axis. Accordingly a respective force-controlled setup had to be designed. To simplify the structure of the test bed the gusset plate was rotated such that the force can be applied in vertical direction. A respective structure was designed and manufactured. The model and a photograph of the test bed are shown in figure 17.

The tests are still in progress. Therefore results of the fatigue tests cannot yet be presented here.

8 Conclusions

With respect to the assessment of lifetime expectancies of steel railway bridges, fatigue is one of the most important failure modes that has to be considered. In engineering practice the remaining lifetime of an existing structure is usually estimated based on numerical analyses according to respective guidelines. In some cases the required proofs cannot be obtained by standard numerical procedures that are based on several assumptions. Some guidelines such as [2] allow to include also experimental investigations into the assessment process.

The presented study shows one possible approach to combine numerical and experimental methods within an improved fatigue assessment of an existing railway bridge. The stages of the presented approach can be summarized as follows:

1. Creation of a numerical global model of the structure

2. Simulation of respective standard loading situations and subsequent stress analyses

3. In case of non-satisfied numerical proofs – extension of the investigations by experimental investigations:

- numerical modal analysis for the validation of the numerical model (that should be updated if it does not represent the real dynamic behaviour sufficiently well)
- experimental estimation of the real loading (axle loads)
- Application of realistic loads within the numerical investigations that can be performed at levels of increasingly refined models
- Control of growth of an existing crack by structural health monitoring

Which of the proposed steps should be applied depends on the individual situation. While in some cases a refinement of the assumed loading situation may already improve the results, the permanent control of an existing crack may lead to a situation where some damage is accepted without a reduction of safety.

The performance of laboratory fatigue tests of specific details can of course not become part of a practical methodology that is regularly applied. However, it is expected that the existing knowledge about the fatigue behaviour of details, for which it is difficult to select an appropriate notch case from codes, can be improved by fatigue tests.

Acknowledgements

The research presented here has been performed within the European research project *Fatigue damage control and assessment for railway bridges* (FADLESS) that has been supported by the European research fund for coal and steel (RFCS), which is highly appreciated. Furthermore it is acknowledged that parts of the equipment that has been used for the presented experimental investigations was purchased with the financial support of the European fund for regional development.

References

[1] EN1993-1-9, "Eurocode 3: Design of Steel Structures, Part 1-9: Fatigue", CEN: Brussels, Belgium, 2004.

[2] Richtlinie 805, "Tragsicherheit bestehender Bauwerke", Deutschen Bahn AG, Germany, 2002.

[3] SIA 269, "Grundlagen der Erhaltung von Tragwerken", Swiss Society of Engineers and Architects, 2011.

[4] B. Peeters, G. De Roeck, "Reference-based stochastic subspace identification for output-only modal analysis", *Mechanical Systems and Signal Processing*, 13 (6): 855–878, 1999.

[5] E. Reynders, M. Schevenels, G. De Roeck, "MACEC: A Matlab toolbox for experimental and operational analysis", Report BWM-2008-07, April 2008.

[6] V. Zabel, M. Brehm, S. Ahmad, L. He, G. De Roeck, "Experimental and numerical investigations of the global dynamic behaviour of a steel railway bridge", in C. Könke (Editor), *Proc. of the D-A-CH-Tagung 2011: Erdbebeningenieurwesen und Baudynamik*, pages 297–308. DGEB, 2011.

[7] Richtlinie 804, "Eisenbahnbrücken (und sonstige Ingenieurbauwerke) planen, bauen und instand halten", Deutschen Bahn AG, Germany, 2010.

[8] Krupp, *www.eisenbahnfieber.de*, Krupp, Udo, 2010, URL `http://www.eisenbahnfieber.de`.

[9] A. Steimel, *Elektrische Triebfahrzeuge und ihre Energieversorgung*, Oldenbourg Industrieverlag, Munich, 2nd edition, 2006.

[10] A. Taras, R. Greiner, "Development and Application of a Fatigue Class Catalogue for Riveted Bridge Components", ECCS TC6 Reports, 2009.